Nanoscale

Peptoid-Directed Assembly of CdSe Nanoparticles

SCHOLARONE™
Manuscripts

Peptoid-Directed Assembly of CdSe Nanoparticles

Madison Monahan[a], Bin Cai[b], Tengyue Jian[b], Shuai Zhang[b,c], Guomin Zhu[b,c,] Chun-Long Chen[b,d], James De Yoreo[a,b,c], Brandi M. Cossairt[a]*

[a]Department of Chemistry, University of Washington, Box 351700, Seattle, WA 98195-1700.
[b]Physical Sciences Division, Pacific Northwest National Laboratory, Richland, WA 99354.
[c]Department of Materials Science and Engineering, University of Washington, Seattle, WA 98195-1700.
[d]Department of Chemical Engineering, University of Washington, Seattle, WA 98195.
*cossairt@uw.edu

Abstract.
The high information content of proteins drives their hierarchical assembly and complex function, including the organization of inorganic nanomaterials. Peptoids offer an organic scaffold very similar to proteins, but with a wider solubility range and easily tunable side chains and functional groups to create a variety of self-assembling architectures with atomic precision. If we could harness this paradigm and understand the factors that govern how they direct nucleation and assembly of inorganic materials to design order within such materials, new dimensions of function and fundamental science would emerge. In this work, peptoid tubes and sheets were explored as platforms to assemble colloidal quantum dots (QDs) and clusters. We have successfully synthesized CdSe QDs with difunctionalized capping ligands containing both carboxylic acid and thiol groups and mixed them with maleimide containing peptoids, to create an assembly of the QDs on the peptoid surface via a covalent linkage. This conjugation was seen to be successful with peptoid tubes, sheets and CdSe QDs and clusters. The particles were seen to have a high preference for the peptoid surface but non-specific interactions with carboxylic acid groups on the peptoids limited control over QD density via the maleimide conjugation. Replacing the carboxylic acid groups with methoxy ethers allowed for control over QD density as a function of maleimide concentration. ^{1}H NMR analysis demonstrated that binding of QDs to peptoids involved a subset of surface ligands bound via the carboxylate functional group, allowing sulfur to bind via covalent linkage to the maleimide. Overall, we have shown the compatibility and control of CdSe-peptoid interactions via a covalent linkage with varying peptoid structures and CdSe particles to create complex hybrid structures.

Introduction.

Nature has perfected the coupling of discrete building blocks into complex hierarchical architectures to elicit distinct functionality. For this reason, synthetic chemists have sought versatile, scalable, and predictive platforms for accessing hierarchy[1-5]. Hybrid materials based on the combination of highly designable organic or biomolecular templates and functional inorganic building blocks are gaining momentum because of their optoelectronic and catalytic potential through synergistic interactions between the individual components of the material. Considerable work has been dedicated to understanding the side chain chemistry in block co-polymers to design materials with specific properties[6-10]. Additionally, protein design and 3D modeling have evolved to allow a great deal of control in directing biological structures, resulting in an organic lattice that is known with atomic precision[11-14]. By using individual subunits, where both the inorganic and organic components are known with atomic precision and can be tuned with

atomic specificity, highly complex, compatible, and stable systems with new structures and properties can be designed.

Peptoids (or poly-N-substituted glycine) are highly tunable sequence-defined biomimetic building blocks, similar to peptides but lacking the amide hydrogen, allowing for a wider range in solubility and generating diverse and robust self-assembled nanostructures that are not readily achieved by peptide self-assembly[15]. Peptoids have been highly engineered and deeply studied to understand the self-assembled structures, their ability to nucleate and control the shape of inorganic particles, and how the side chains and periodicity alter these interactions[16-22] One of the most common designs of self-assembling peptoids is a di-block sequence consisting polar and nonpolar domains, such as those shown in **Fig. 1a,b**. Such di-block self-assembling peptoids have been demonstrated to form highly crystalline nanotubes or membrane-mimetic 2D nanosheets (**Fig. 1a-e, g-j**), depending on the sequence in the hydrophobic region[23-25]. For both sheets and tubes, the peptoids form an interdigitated bi-layer in which the peptoids stack in alternating "upward"- and "downward"-pointing rows with the internal, hydrophobic regions stabilized by π stacking of the phenyl rings, and the hydrophilic regions exposed at the surface for interaction with the bulk aqueous solution (**Fig. 1d,e**)[23,24]. For the sequence used here, the bilayer thickness is 3.5- 4 nm depending on solution pH and salt concentration. Using similar peptoid sequences, these nanostructures have been shown to be stable over a range of pH values and temperatures[24]. The high stability of these peptoid nanosheet and nanotube scaffolds along with their easily functionalized hydrophilic regions results in an ideal structure for templating inorganic materials to access hybrid assemblies.
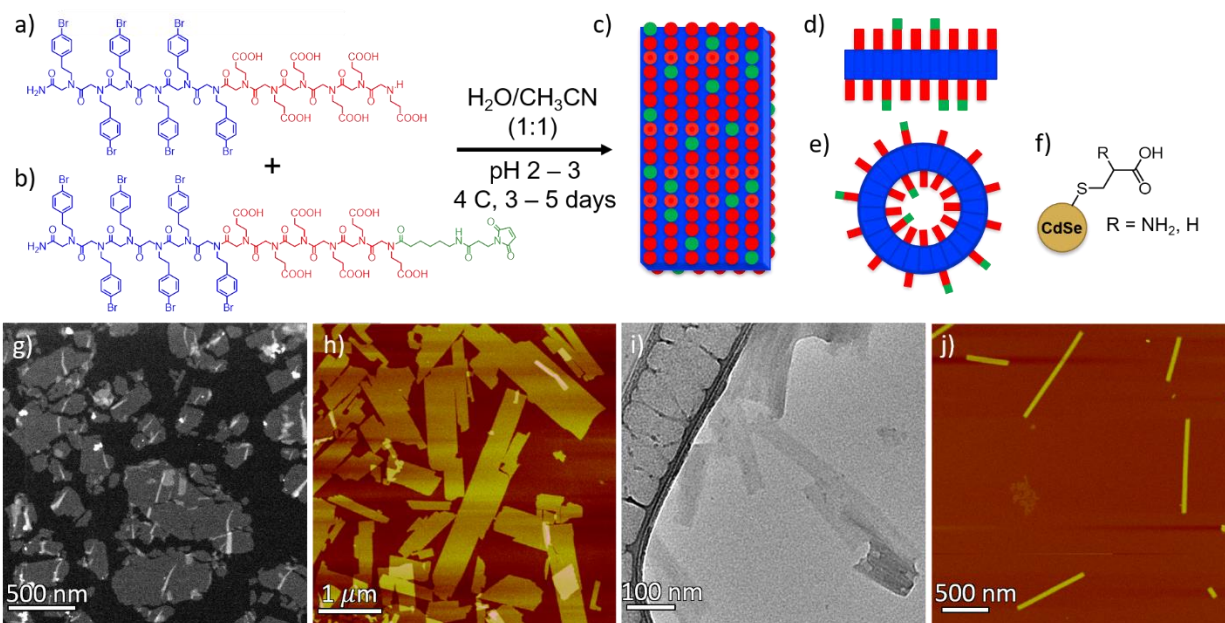
Figure 1. Diblock peptoid monomers (a) contain a hydrophobic region (blue) and a hydrophilic region (red). A mix of standard (a) and functionalized (b) monomers are mixed during assembly to give a random distribution of maleimide functionalization on the surface (green, c). The hydrophobic regions of the monomers reside internally (blue) and hydrophilic regions reside externally (red) in the resulting interdigitated bi-layer peptoid sheets and tubes (d,e). CdSe particle (gold) attachment via the maleimide on the peptoid structure and a thiol in the capping ligand on the nanoparticle surface (f). Transmission electron microscopy (TEM) and atomic force microscopy (AFM) images of self-assembled peptoid sheets (g,h) and tubes (i,j). The

unstained peptoids can be seen clearly via STEM (g) but require slight defocus to be resolved in bright field imaging (i).

In this work, we examine CdSe quantum dots (QDs) (**Fig. S1a**) and magic size clusters (MSCs) (**Fig. S1b**) capped with difunctionalized ligands containing carboxylic acid (-COOH) and thiol (-SH) moieties (**Fig. 1f)** assembled in solution onto maleimide functionalized peptoid sheets and tubes, like those in **Fig. 1g-j**. CdSe nanoparticles have a long history of use in combination with biological and biomimetic systems, and have been shown to be both water soluble and stable under a variety of conditions and with a variety of surface chemistries[26-30]. Additionally, there has been significant work done on tuning the optoelectronic properties of CdSe nanoparticles by changing their size, morphology, and capping ligands[31-34]. The use of both MSCs and QDs results in two distinct systems that have similar compositions and chemistries but different spectroscopic properties due to their size and structural differences[35,36]. Working with sheet-forming peptoids and QDs, the compatibility of the two systems is explored by altering the capping ligands of the particles and the side chains of peptoid backbones to create a system that is stable under the mildly acidic, aqueous conditions required for peptoid stability. We show control over the density of QDs on the surface of peptoid sheets as a function of maleimide percentage within the sheet. The system is proven generalizable by creating conjugates with peptoid nanotubes as well as extending the methodology to produce conjugates with atomically precise CdSe clusters. Finally, the QD and peptoid interactions are probed using NMR spectroscopy and different component compositions to determine the operative binding mechanism.

Results and Discussion.
Conjugation of peptoid structures and CdSe particles.

To create viable conjugation with the peptoid structures, the quantum dots must have complimentary functionalization and compatible solubility. For our system, we must design quantum dots that are both soluble in water and have high selectivity and reactivity to maleimide. Maleimide reacts under appropriate conditions with thiols to create a covalent C—S bond[37]. Conjugation between inorganic and organic units has been demonstrated using maleimide-thiol chemistry, but the approach is most commonly implemented with the maleimide functionalizing the inorganic particle and complementary cysteines positioned within the organic framework[38-40]. There are a few examples of functionalizing an inorganic particle with sulfur, either by conjugation of sulfur within the inorganic core or using a capping ligand that contains multiple thiols to maintain the sulfur interaction with the core and bind the maleimide[41-44]. The particle surface must be ligated by a molecule that both contains a binding group to attach to the particle and an additional functional group to bind to the peptoid. Cysteine has been well-studied for the synthesis of water soluble and biocompatible QDs that interact favorably with proteins, commonly with other cystines to create a disulfide bond or via electrostatics[45,46]. Synthesis of cysteine capped CdSe has been reported extensively, with relatively mild aqueous conditions yielding well defined clusters and QDs.

Based on existing precedent, cysteine-capped CdSe (cys-CdSe) QDs were synthesized (**Fig. S1a**) under basic conditions (pH 12) and were stored at pH 8 to limit disulfide formation that readily occurs at pH greater than 8.5[47]. Peptoid sheets and tubes were co-assembled from different proportions of monomers bearing six polar residues (N-(2-carboxyethyl)glycine) and six nonpolar residues (N-[2-(4-bromophenyl)ethyl]glycine for sheets or N-[2-(4-

3

bromophenyl)methyl]glycine for tubes). The monomers were terminated with either a standard NH terminus or a maleimide group with the intention of creating nanosheets and nanotubes with highly tunable maleimide density for covalent attachment of QDs (**Fig. 1a,b**). Notably, similar peptoid sheets have been demonstrated to remain stable under a large range of conditions including basic pH values up to pH 10[23]. Acidic conditions can lead to etching of QDs that can lead to shrinkage and even destabilization depending on the duration of exposure and the exact pH. For the above reasons, conjugation was performed at pH 7 with a 1 h incubation time using a 0.17 mM solution of peptoid sheets (concentration determined by individual peptoid monomers used for assembly) and a 4.2 μM QD solution. After incubation, the material was used crude to prepare the sample for analysis by electron microscopy and AFM.

TEM was the main method of characterization, with scanning (S)TEM used to identify peptoid sheets and standard bright field methods employed to analyze particle density. TEM analysis showed a strong preference for QDs to bind to the peptoid sheets and tubes with few to no free QDs observed away from the peptoid structures (**Fig. 2a-d**). Particle identity was confirmed using energy dispersive X-ray (EDX) analysis to identify Cd and Se in the sample (**Fig. S2a**). No Cd or Se peaks were observed with peptoids alone (**Fig. S2b**). The QDs remained stable with an average size of 2.82 $\pm$ 0.30 nm, but the peptoid sheets appeared to destabilize slightly under the conjugation conditions. Before conjugation, peptoid sheets averaged a few hundred nanometers in length, some as large as a micron in length, with straight, well defined edges and a rectangular shape (**Fig. 1g,h**). After conjugation, peptoid sheets appeared to have rounded edges and were significantly smaller with an average length of 50 nm (**Fig. 2a,b**). It is probable that the change in morphology is limited to the edges of the peptoid sheets, with the crystalline nature of the peptoids preserved due to the primary sheet structure remaining intact, however, this cannot be confirmed under standard imaging conditions. The observed morphology changes in the peptoid sheets could be due to the increase in pH upon conjugation, interactions with the QDs themselves, or a result of imaging with an electron beam (see below for discussion following investigation by AFM).
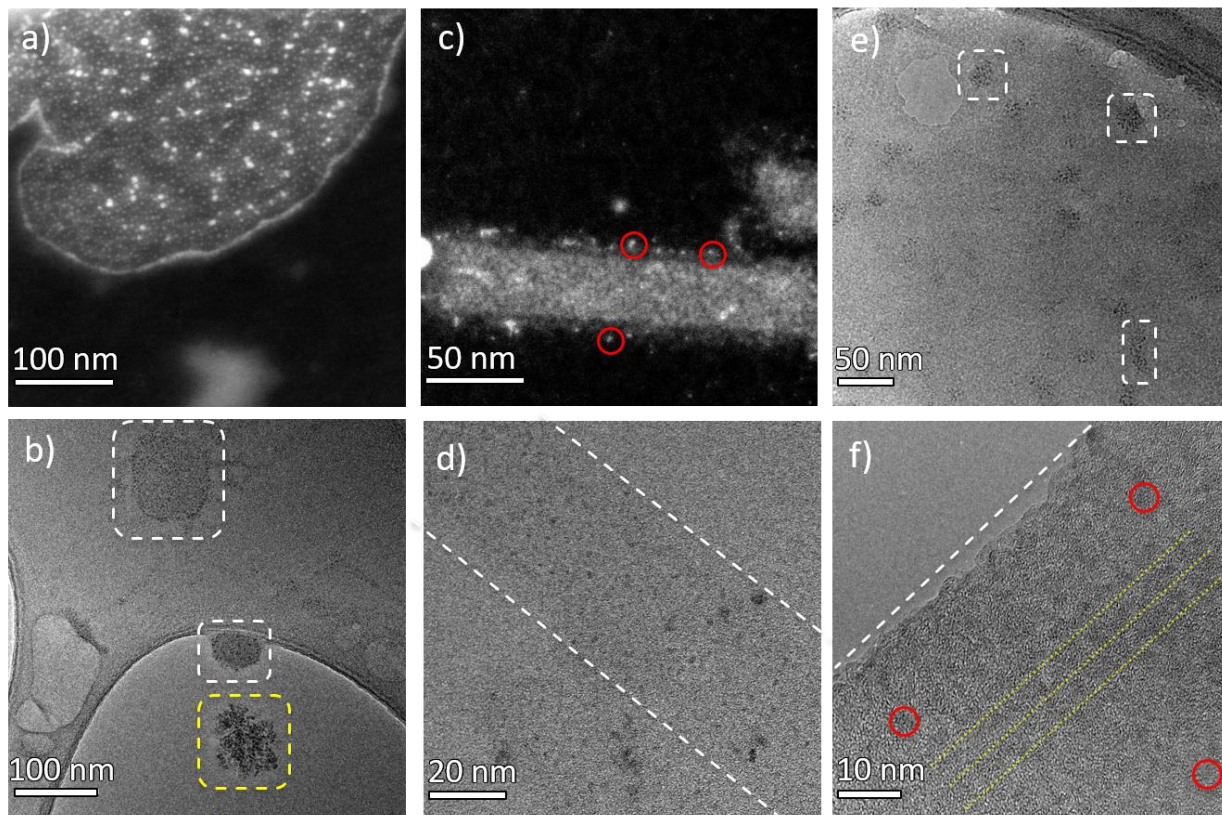
Figure 2. (a, b) Cys-CdSe QDs exhibit a strong preference for binding to maleimide-functionalized peptoid sheets (a) but destabilization of the sheets is seen by the smaller sheet sizes than observed in the absence of the QDs, as well as rounding of the sheet edges (b, white dashed line). (b). QD aggregates unassociated with peptoid sheets can sometimes be seen (yellow dashed line in b), recognizable by their dendritic morphologies and irregular particle distributions. (c) STEM image of peptoid tubes conjugated with CdSe QDs, seen along the tube edges (red circles). (d) Standard TEM shows that the QDs have a high preference for the tubes (white dashed lines), with uniform distribution. (e) CdSe clusters conjugated with a peptoid sheet (white dashed lines) with significant shrinkage of the sheets observed. (f) Tubes with clusters (red) exhibiting linear trends (yellow dotted lines) parallel to the tube edge (white dashed line), consistent with the interdigitated row-by-row, bi-layer structure of the peptoid tubes (**Fig. 1c-e**).

To test the versatility of the hybrid peptoid-CdSe system, conjugation was performed with atomically precise cys-CdSe clusters characterized by a lowest energy electronic transition at 420 nm[48]. We find that CdSe clusters have reactivity comparable to that of their QD counterparts but are less robust to a variety of conditions. Conjugation was performed under standard conditions, replacing the QDs with clusters using the same total concentration (4.2 μM). Clusters showed the same strong preference for binding to the sheet surfaces (**Fig. 2e**) and maintained their structural integrity based on their observed sizes (~2 nm). Again, the observed peptoid sheets were small and rounded after conjugation.

Peptoids have also been shown to assemble into nanotubes by changing the length of the carbon side chain in the hydrophobic region, with an average nanotube being 40 nm in diameter and up to a micron in length (**Fig. 1a,e**). Using peptoids with the same hydrophilic monomer sequence as for the sheet forming sequence, but with a tube generating hydrophobic sequence

(containing one less carbon on the side chain), conjugation was performed with both cys-CdSe QDs and clusters at pH 7. Both the clusters and QDs showed a strong preference for the peptoid tube surface. The QDs and clusters are presumably also present inside the pore of the tubes but diffusion within the tube is likely limited by the irreversible binding to maleimide. However, the tubes did not show any signs of destabilization upon conjugation with the particles, in contrast to the destabilization seen with the sheets. This high degree of stability could be due to the rigidity of the tube structure relative to the sheets and may suggest that by altering the peptoid monomer, specifically the side chains to create stiffer sheets, better sheet stability could be obtained. Interestingly, alignment of the clusters parallel to the tube edge can be seen on the tube surface (yellow dotted line, **Fig. 2f**) consistent with the interdigitated row-by-row, bi-layer structure of the peptoid tubes (**Fig. 1e**). The same ordering was not observed in the case of the QDs, which we suspect may be a result of their inherent polydispersity and large size (**Fig. 2c,d**).

Creating a compatible system.

As mentioned previously, peptoid sheets should remain stable at pH values up to pH 10 but this structural robustness is reliant on peptoid sheets being adequately crystalline[23,24]. Therefore, we sought different conjugation conditions to create a compatible and reproducible system. Conjugation was performed at pH 6 with cys-CdSe QDs to emulate conditions used for long-term storage of the peptoid sheets. Under slightly acidic conditions, the sheets retained their micron size and rectangular shape but the QDs were observed to aggregate with unsuccessful conjugation as there was no observed preference for QDs to bind the peptoid sheets (**Fig. S3**). Based on the pKa values of cysteine, operating at pH 6 likely results in a zwitterion, which may decrease QD solubility and lead to the observed aggregation[49].

A comparable bifunctional ligand to cysteine, mercaptopropionic acid (MPA) (**Fig. 1f**, R=H), has been used in the QD literature to solubilize QDs under acidic conditions[49-51]. Additionally, MPA has a similar structure to cysteine, but without the amine substituent which should limit pH related solubility issues and be less favorable for disulfide formation[47]. CdSe QDs were synthesized with MPA as the capping ligand (MPA-CdSe) under the same conditions as cys-CdSe. After purification, the QDs were titrated with HCl, starting at pH 7, down to pH 4 while monitoring the absorbance and photoluminescence. MPA-CdSe retained their well-resolved absorption features down to pH 5.5 after which the excitonic transitions began to broaden the absorption peaks with an increase in scattering (**Fig. S4a**). After incubation overnight at pH 6, MPA-CdSe remained stable with an average size of 2.77±0.70 nm without significant etching as observed by TEM (**Fig. S4b**).

Conjugation using MPA-CdSe QDs showed a strong preference for QD association with the peptoid surface. The peptoid sheets better maintained their structure under these conditions than under those used with cys-CdSe, however, the sheets still showed rounding of their edges. This effect has two possible sources. The first is destabilization of the sheet edges due to interactions between the QDs and the peptoids exposed at the edges and due to conditions under which conjugation was performed. The second is the binding of a single QD to multiple maleimide units on the peptoid. We expect that the majority of the MPA is bound to the QD surface through thiolate ligation, with the carboxylic acid exposed to solution based on literature precedent for these systems[52,53]. However, under acidic conditions, the QD surface is likely to have some fraction of exposed thiol that is available for interaction with the maleimide on the peptoid (see below for additional analysis of the binding mechanism using NMR spectroscopy). Additionally, the peptoid monomers contain a relatively long hydrophilic region, enabling QDs

bound near the edge of the peptoid sheet to interact with a MPA on the opposite peptoid surface and cause rounding of the edge.

The extent of destabilization has been seen to vary between samples and appears to be somewhat correlated with pH changes and maleimide concentration. Peptoid sheets are typically assembled under acidic conditions and stored around pH 2-3, but they have been shown to be stable to and assemble at pH 10[23,24]. Conjugation is performed at pH 6-7 to promote QD stability and this increase in pH could contribute to changes in peptoid sheet morphology. The peptoids used in this system were incubated overnight at pH 7 without QDs present and were observed to maintain their larger sheet size but still showed rounding of the edges (**Fig. S5**). Conjugation above pH 8 still shows a strong preference for QD binding to the peptoid surface, but further evolution of the peptoid morphology to fibril like structures is observed (**Fig. S6**). Incidentally, the percentage of peptoids displaying a maleimide group is controlled at the time of sheet assembly by the relative concentrations of -maleimide and -COOH terminated monomers. Sheets containing 20, 50, and 80% maleimide-terminated monomers were conjugated with MPA-CdSe QDs and analyzed. The peptoid sheets retained their generally rectangular structure in the case of 20% maleimide but begin to show large amorphous structures at 50 and 80% maleimide (**Fig. S7**). Maleimide is known to be highly selective for thiols under a range of conditions, but it has been shown to react with amines over thiols at pH values above 7.5[54]. If the solution used for conjugation becomes too basic or there are local concentrations at the peptoid sheet surface of higher pH, the maleimide could react internally with the peptoids themselves to create an amorphous structure.

Another possible source of the reduced size and rounded edges is the interaction of the QD-functionalized peptoid sheets with the electron beam during TEM imaging. Although, if this is a source of the effect, it must occur upon initial exposure, because no evolution of peptoid sheet morphology was observed during prolonged TEM imaging. To determine if the electron beam contributed to destabilization, AFM was performed on two identical TEM grids containing QD-functionalized methoxy ether peptoid sheets (structure discussed below), one exposed to the electron beam and one not. AFM images of the beam exposed grid showed slightly shrunken and rounded flake-like sheets with QDs attached, consistent with the TEM images (**Fig. 3a-d**). In contrast, the unexposed grid contained large peptoid sheets with straighter edges and QDs on the surface (**Fig. 3e-f**). However, ruling out the presence of some amount of smaller, rounded sheets is not possible give the inherent limit on the field of view for which the range of heights is small enough to resolve ~4 nm high sheets by AFM. Further supporting the hypothesis that the electron beam is at least a partial source of destabilization, electron beam exposure of maleimide-free peptoid sheets in the presence of unbound QDs did not result in destabilization; rather well defined, rectangular peptoid sheets were observed in TEM (**Fig. S8**). The lack of degradation upon prolonged exposure and the observation of fracturing only when the QDs were bound to the peptoid surface suggests that, while degradation induced by the electron beam may occur important, it may not be the only source of destabilization. Rather the chemical effects associated with QD-peptoid conjugation and discussed above may also be a factor. Overall, peptoid destabilization appears to be an unavoidable result of conjugation with nanoparticles but can be minimized by remaining at moderate maleimide concentrations, operating under acidic conditions, and limiting electron beam exposure (**Fig. S9**).
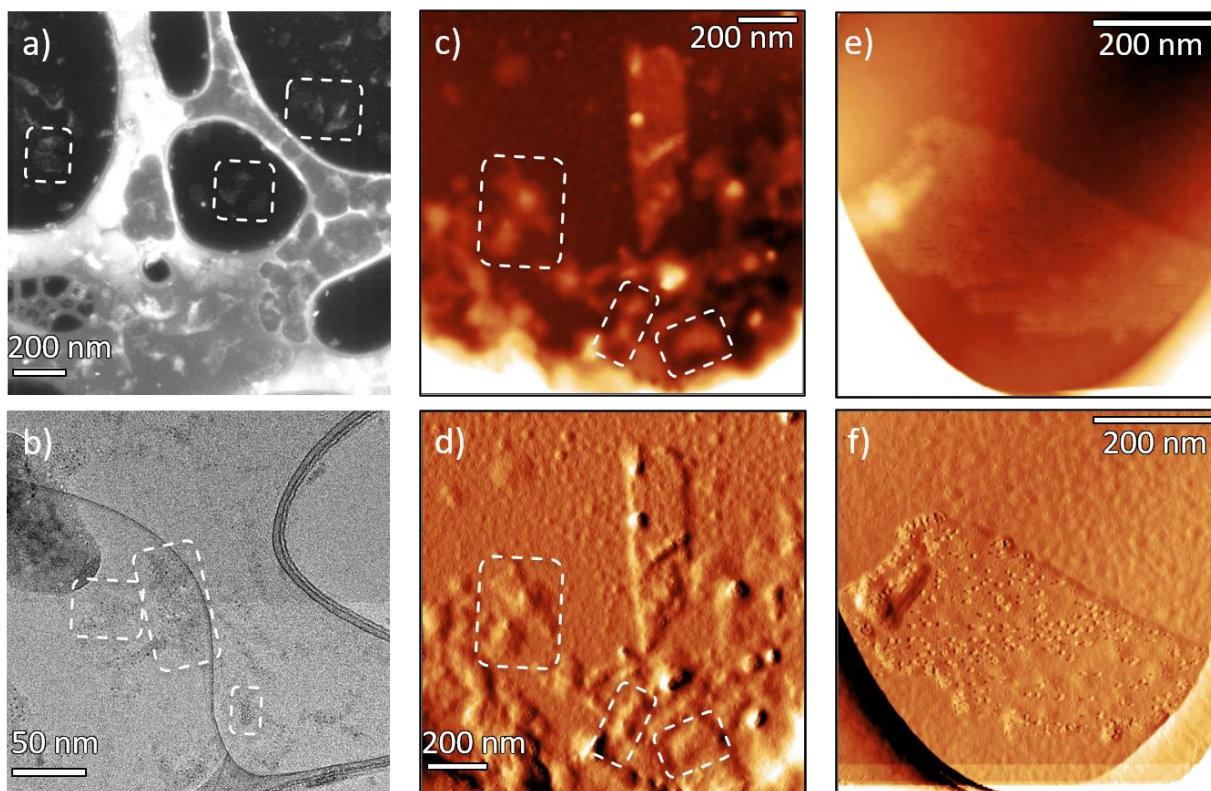
Figure 3. (a,b) 10% maleimide-functionalized peptoid sheets with MPA QDs on a lacey carbon grid imaged via STEM (a) and bright field TEM (b) showing small, flake-like peptoid sheet-QD conjugates (white dashed line). (c,d) The same TEM grid imaged via AFM showing primarily small peptoid sheet-QD conjugates with a few large, intact sheets. (e,f) AFM of 10 % maleimide-functionalized peptoid sheets with MPA QDs on a lacey carbon grid without exposure to the electron beam, indicating conjugation between QDs and peptoids occurs without destabilization or shrinkage of the peptoid sheets and, thus, electron-beam exposure is the source of these effects.

CdSe conjugation density depends on maleimide content.

To test our ability to control QD density on the peptoid sheets, experiments were performed with cystine-capped CdSe QDs at pH 7 with peptoid sheets assembled from 10, 50, and 100% maleimide-terminated peptides. Strong preference for QDs to bind to the peptoid sheets with few QDs found independent of the sheets was observed for all cases (**Fig. S10**). Moreover, all samples also showed complete saturation of the peptoid surfaces with QDs with no QD density difference regardless of the degree of maleimide functionalization. To understand this result, consider the impact of carboxylic acid groups in the peptoid monomers. With the standard di-block peptoid monomer, the hydrophilic region is functionalized with carboxylic acid sidechains to ensure good solubility. Carboxylates are known to act as effective ligands to stabilize QD surfaces[52,53]. We postulate that the observed saturation of the peptoid sheet surface is likely due to non-specific interactions of the QDs with the carboxylates from both the maleimide-functionalized and non-functionalized peptoid monomers. To block these non-specific interactions and maintain the hydrophilicity of the peptoid monomer, we replaced the carboxylic acid side chains with methoxy ethers (**Fig. 4a**), thus ensuring the only favorable peptoid-QD interaction occurs via the maleimide terminus.
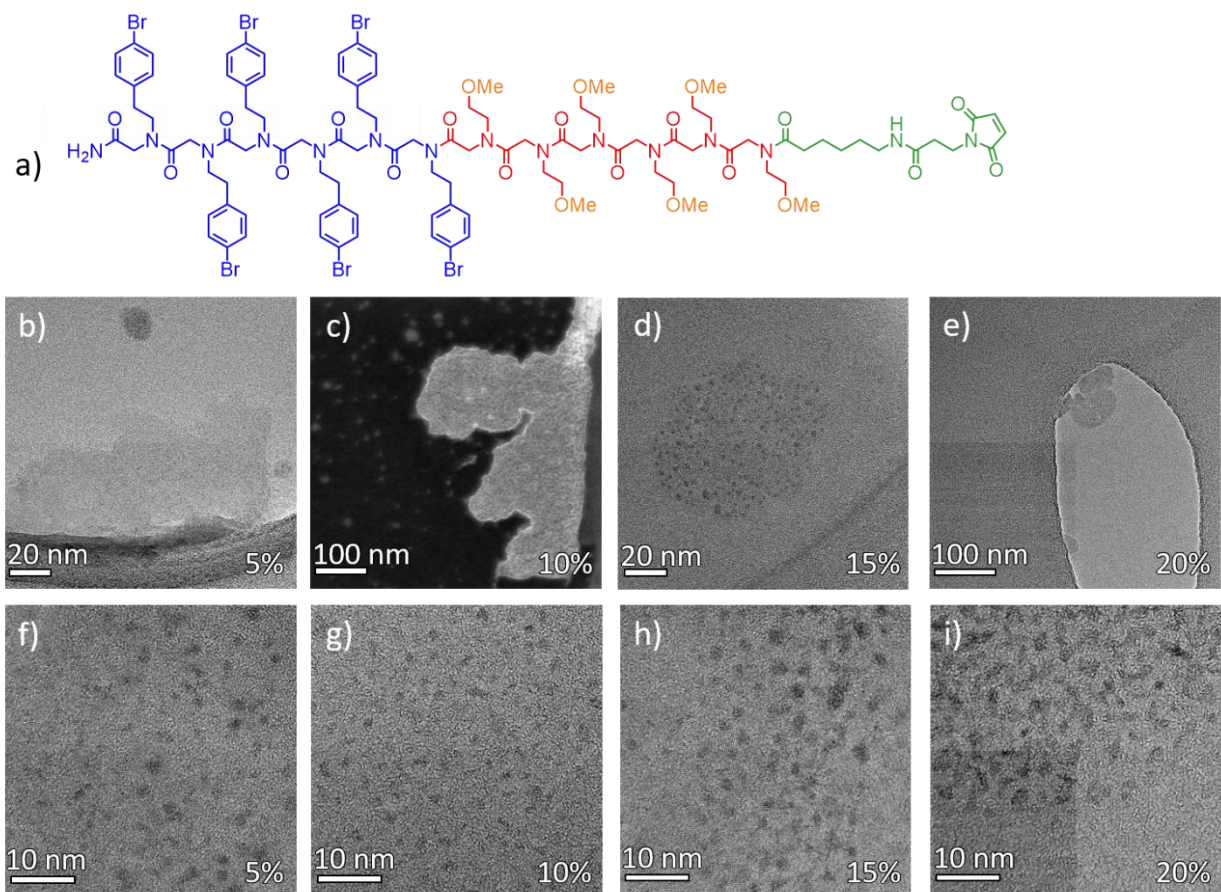
Figure 4. (a) Methoxy ether functionalized peptoid monomer used to eliminate non-specific QD interactions with carboxylic groups of the peptoid backbone. (b-i) Conjugation of MPA QDs with methoxy ether peptoid sheets at pH 6 with (b,f) 5, (c,g) 10, (d,h) 15, and (e,i) 20% maleimide. Peptoid sheets still show some rounding and destabilization (d,e) but maintain a larger sheet size at pH 6 than at pH 7 (compare b and c to Fig. 2b). QD density on the sheet surface increases with maleimide percentage with slight etching of the QDs from 2.82 ± 0.30 nm to 1.78 ± 0.28 nm (f-i).

Conjugation of methoxy ether peptoid sheets and MPA-CdSe QDs was carried out at pH 6. For all samples, MPA-CdSe QDs are seen to maintain their crystallinity, but are etched slightly, exhibiting an average loss of 1 nm in diameter after conjugation (**Fig. 4b-i**). Particle shrinkage likely arises from a combination of the mildly acidic conjugation conditions and interactions with the peptoids, as minimal etching is observed when the particles are incubated at pH 6 alone. Successful peptoid functionalization via maleimide was observed for maleimide concentrations ranging from 2.5 to 20%. The particle size after conjugation averaged 1.78 nm with a uniform distribution across the peptoid sheets except in the case of 2.5% maleimide functionalization, for which QDs were localized at the edges of the peptoid sheets (**Fig. S11**). For maleimide functionalization of 5 to 20%, the percent coverage by area of QDs on the sheets — determined by measuring the diameter of every QD on a fixed area of peptoid sheet and dividing the total QD area by the total peptoid area — tracks with the percent maleimide functionalization for a given sample (**Table 1**).

The maleimide location is generally thought to be random within the orderly packed peptoid rows in each sheet and should be equally distributed on the top and bottom faces. Thus, QDs should exhibit similar coverages on both sides. The calculated percent coverage assumes that all QDs are on one side of the peptoid sheet (i.e. – only one side is in focus in an image), but, due to the relatively low contrast of carbon-based materials in bright field TEM and the sheets only being 3-4 nm thick, it is likely that QDs from both sides of the peptoid sheets are seen in a given image. To determine whether this is the case, AFM analysis was repeated using 10% maleimide-functionalized sheets for which TEM imaging gave 11.1% coverage. AFM imaging gave a QD coverage of only 2.9% (**Table 1**). If one assumes TEM images record QDs on both sides of the sheet, then this value represents more than half the coverage determined by TEM, appearing to confirm that the peptoid sheets are thin enough to see QDs above and below the sheet in the TEM. However, because tip convolution associated with the AFM measurement of particles renders the apparent size to be significantly larger in AFM then TEM — 3.0 nm vs. 1.9 nm, the calculated number densities are more disparate giving values per face of the peptoid sheet that differ by a factor of 5 (2×10^{-2} QDs/nm^{-2} vs 0.4×10^{-2} QDs/nm^{-2}). The difference in QD number density seen in TEM vs AFM may be the result of batch-to-batch variability, as the sheets used to determine the coverage by TEM came from a different synthesis run than those used for in AFM. For a more direct comparison, a sample of QD conjugated peptoids with 10% maleimide was first analyzed by TEM with AFM analysis immediately following on the same sample. The QD number density was more consistent between these two samples, differing only by a factor of two with the TEM and AFM measurements giving values of 0.9×10^{-2} QDs/nm^2 vs 0.4×10^{-2} QDs/nm^2, respectively.

Table 1. Analysis of MPA CdSe QDs on peptoid sheets of varying maleimide percentage. The percent of sheet surface covered assumes all QDs seen are on one side of the peptoid sheet. QD diameter was determined via TEM analysis for all samples and percent coverage was determined via TEM analysis unless otherwise noted.

Percent maleimide	Percent covered	QD average diameter (nm)	QD/peptoid area ($\times 10^{-2}$ nm^{-2})	QD/peptoid area ($\times 10^{-2}$ nm^{-2}) accounting for both sides of peptoid
5%	5.9	1.8	3.2	1.6
10% (sample A)	11.1	1.9	4.0	2.0
10% (sample B)	12.6	3.0	1.8	0.9
10% (sample B via AFM)	2.9	3.0	0.4	N/A
15%	14.7	1.7	6.2	3.1
20%	19.6	1.8	7.6	3.8

Determining binding mechanism.
        The specificity of MPA-CdSe QD binding to maleimide-functionalized peptoid sheets could be driven by multiple binding mechanisms. The QDs could adhere to the surface either via electrostatic interactions or via the formation of a covalent bond to a moiety on the peptoid

surface. Thiolate groups are known to bind more strongly than carboxylate groups to a CdSe QD surface, suggesting that a reasonable model for the QD surface is majority thiolate coordination to the CdSe with the carboxylic acid moiety exposed to the bulk solution[52,53]. However, if the thiol is required for maleimide conjugation, we would then expect that ligand rearrangement to a carboxylate-bound form is a requirement. Moreover, while a preference for carboxylate binding to the surface over that of thiolate is improbable at high pH values, at lower (neutral or acidic) pH values the thiolate protonates and binds much less strongly to the CdSe surface[55]. Also, conjugation may occur via direct bond formation between the chalcogenide core of the particle and the maleimide, as has been observed in the case of MoS_2 and WS_2[41]. To test for covalent bond formation and isolate the mechanism of biding, we performed several control experiments and followed them by TEM and/or NMR spectroscopy as described below.

First, to confirm that the observed specificity was dependent on covalent bond formation with the maleimide, as suggested by the density dependence study, conjugation of MPA-CdSe QDs was attempted at pH 6 with methoxy ether substituted peptoid sheets containing 0% maleimide. TEM analysis showed QDs randomly scattered across the sample with slight aggregation (**Fig. 5a**), as is common in images of the QDs alone (**Fig. 2b**, yellow dashed line). Peptoid sheets retained their micron size with well-defined, straight edges and with little to no QD coverage for any given sheet. The lack of QD binding to the peptoid sheets with 0% maleimide incorporation confirms that the preference for the peptoid surface is driven by covalent bond formation with the maleimide and is not due to electrostatic interactions between the sheet surface and the QDs.

To determine the role of thiol in the conjugation, CdSe QDs were synthesized with s-methyl-l-cysteine as the capping ligand to create a carboxylate-capped surface and a solution-facing thioether group (**Fig. S12**). Notably, previous studies of the binding of cysteine to CdSe nanoparticles show that while the amine can help stabilize the particle surface, it will not act as the primary binding group[56]. Furthermore, previous studies of maleimide conjugation have not revealed complicating interactions between maleimide and carboxylate functional groups. Conjugation was performed under standard conditions with 20% maleimide peptoid sheets and analyzed via TEM. As with the 0% maleimide case, no preference was seen for the QDs to adhere to the peptoid surface; QDs were randomly scattered across the sample (**Fig. 5b**). The unsuccessful conjugation indicates that the thiol is vital for maleimide conjugation. Additionally, it suggests that the sulfur is not reactive in its thioether form and therefore it is unlikely that, with the standard thiolate capped QDs, the sulfur maintains its interaction with the QD surface, but, instead, binds to the maleimide.
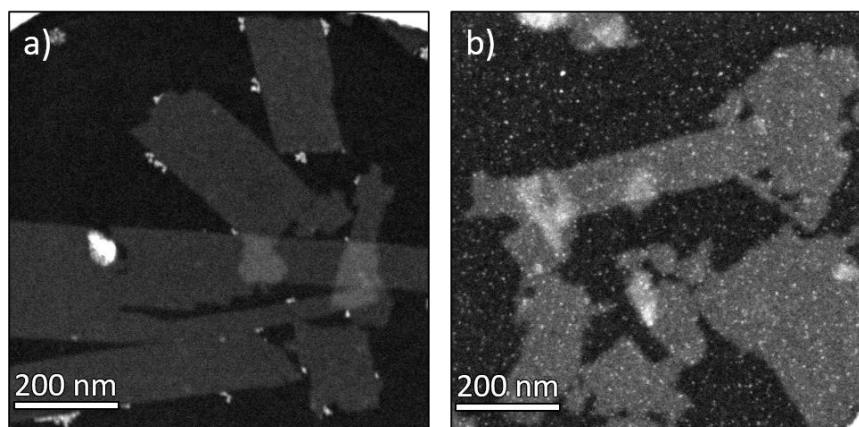
Figure 5. Unsuccessful conjugation of peptoid sheets with 0% maleimide with MPA-QDs at pH 6 (a). Sheets maintain defined rectangular shape and 500 nm length with the QDs aggregated randomly, likely due to drying effects on grid. 20% maleimide sheets with S-methyl-L-cysteine capped QDs and pH 6 (b) showing QDs randomly scattered around the grid with no localization of QDs to the peptoid sheet.

These results support our hypothesis that ligand rearrangement is occurring under the conjugation conditions or that, based on the relative equilibria, some fraction of the ligands are already present on the QD surface in their carboxylate bound form[57]. To further test for ligand rearrangement, $Cd(MPA)_2$ was synthesized from $CdSO_4$ and doubly deprotonated MPA and isolated for titration with a maleimide-containing small molecule surrogate, 6-maliemidohexanoic acid (EMCA), for analysis by ^1H NMR spectroscopy. Prior to EMCA addition, two triplets associated with the MPA are observed at 2.56 and 2.90 ppm. With EMCA addition, the peaks associated with the carbon chain grow in as expected with the resonance associated with the methylene alpha to the carboxylate shifting the most from 2.36 ppm to 2.19 ppm (**Fig. 6**). The singlet associated with the double bond in the maleimide ring is not observed (**Fig. S13**), instead growth of three peaks at 2.75, 3.31, and 4.07 ppm is observed, consistent with binding of the maleimide with the sulfur of the MPA. The expected MPA-maleimide complex should only show two new peaks, but the maleimide ring is well known to be more stable in an open configuration after conjugation with a thiol[58]. Overnight incubation of the solution led to the disappearance of the peak at 4.07 ppm, a concomitant sharpening of the peak at 2.75 ppm, and an increase in the integrated area of the peak at 3.31 ppm. This indicates that initial mixing produces both the open and closed ring conformations, with the open ring species being the majority after incubating overnight. At low EMCA concentration in solution, the peaks associated with MPA protons did not shift upon binding of the maleimide, implying that no ligand rearrangement is needed to bind the maleimide, and thus supporting the presence of a population of MPA bound via the -COOH[57]. At higher EMCA concentrations, peaks shift down field and a distinct set of triplets grow in at 2.54 ppm and 2.92 ppm. The new triplet is both distinct from the original peak and associated with maleimide binding as it integrates 1:1 relative to EMCA in solution (**Table S1**). This observation supports MPA rearrangement in the Cd-complex to bind via the -COOH and free the sulfur for maleimide binding. The downfield shift of the remaining $Cd(MPA)_2$ peaks is likely a result of some mixed ligand environment as rearrangement occurs. The addition of maleimide to $Cd(MPA)_2$ confirms the ability of MPA to form a stable covalent bond with maleimide and supports a population of MPA bound via -COOH to cadmium. While this data suggests rearrangement is plausible at high concentrations of maleimide (> 2 eq. maleimide per $Cd(MPA)_2$), conjugation with the peptoid nanostructures was performed with a low enough maleimide concentration that we believe that it is unlikely rearrangement occurs at the nanoparticle surface. Instead, we envision that accessible maleimide side chains are likely engaged in conjugation by the fraction of MPA bound via the carboxylate.
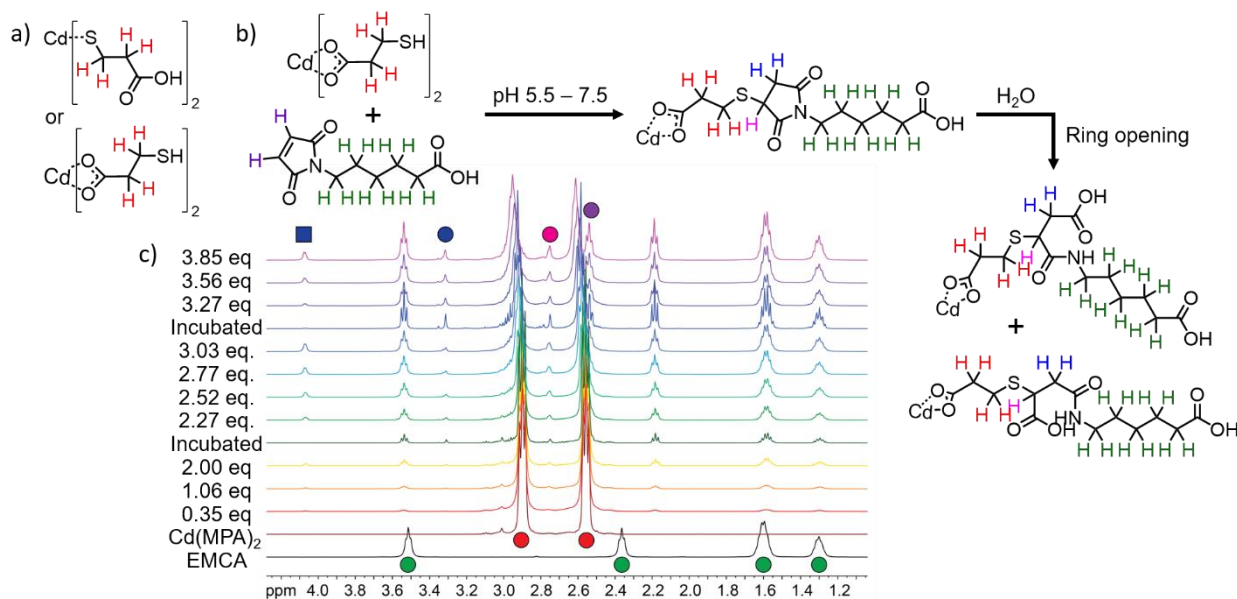
Figure 6. (a) Potential binding modes for MPA to cadmium and (b) the proposed reaction mechanism for Cd(MPA)$_2$ with maleimide. (c) NMR analysis of Cd(MPA)$_2$ with increasing EMCA. EMCA carbon peaks grow in as expected (green), MPA begins to shift after 2 eq. EMCA (red), with a new triplet growing in (purple), and new peaks seen from successful conjugation (blue and pink). The mix of open and closed ring maleimide conformations can be seen with two different hydrogen species representing the hydrogens beta to the sulfur (blue circle and square, respectively).

Conclusions.

Understanding the interactions between peptoid structures and inorganic particles is key in designing compatible components and engineering hybrid composites with unique functionality. In this work, we have demonstrated the use of peptoid materials to template the arrangement of CdSe nanoparticles with control over the QD density based on the percentage of maleimide incorporated into the peptoid structure. We demonstrated the generality of the conjugation by using both peptoid sheets and peptoid tubes and using both CdSe QDs and atomically precise CdSe clusters. By tuning both the organic and inorganic subunits of the hybrid assembly, we have gained insight into the stability and compatibility of the two components and have identified conditions under which we can tune the QD number density. Furthermore, we have identified the operative mechanism governing the selectivity of the particles for the peptoid surfaces with a subset of MPA bound via the carboxylate to the CdSe surface, which allows for direct interaction of the sulfur with the maleimide. By understanding the design principles required to create hybrid assemblies between peptoid structures and CdSe particles, we have established a platform for expanding the structural and compositional diversity of these systems. Finally, we demonstrated exceptionally mild conditions for nucleating CdSe nanoparticles and their compatibility with peptoid structures, opening the possibility of using peptoids as a nucleation platform for CdSe nanomaterials.

Supporting Information.

Corresponding Author.
*cossairt@uw.edu

References.
1. G. Kickelbick, *Hybrid Materials*, 2014, **1**, 39-51.
2. P. A. Gabrys, L. Z. Zornberg and R. J. Macfarlane, *Small*, 2019, **15**, 1805424.
3. Y. Tian, J. R. Lhermitte, L. Bai, T. Vo, H. L. Xin, H. Li, R. Li, M. Fukuto, K. G. Yager, J. S. Kahn, Y. Xiong, B. Minevich, S. K. Kumar and O. Gang, *Nature Mater.*, 2020, **19**, 789–796.
4. J. Snyder, K. Livi and J. Erlebacher, *Adv. Funct. Mater.*, 2013, **23**, 5494–5501.
5. C. Pigliacelli, R. Sánchez-Fernández, M. D. García, C. Peinador and E. Pazos, *Chem. Commun.*, 2020, **56**, 8000–8014.
6. H. Sai, K. W. Tan, K. Hur, E. Asenath-Smith, R. Hovden, Y. Jiang, M. Riccio, D. A. Muller, V. Elser, L. A. Estroff, S. M. Gruner and U. Wiesner, *Science*, 2013, **341**, 530–534.
7. R. M. Dorin, H. Sai and U. Wiesner, *Chem. Mater.*, 2014, **26**, 339–347.
8. X. Zhang, P. Tanner, A. Graff, C. G. Palivan and W. Meier, *J. Polym. Sci. A*, 2012, **50**, 2293–2318.
9. E. J. Robertson, A. Battigelli, C. Proulx, R. V. Mannige, T. K. Haxton, L. Yun, S. Whitelam and R. N. Zuckermann, *Acc. Chem. Res.*, 2016, **49**, 379–389.
10. V. Castelletto, J. Seitsonen, K. M. Tewari, A. Hasan, R. M. Edkins, J. Ruokolainen, L. M. Pandey, I. W. Hamley and K. H. A. Lau, *ACS Macro Lett.*, 2020, **9**, 494–499.
11. C. A. Mirkin, R. L. Letsinger and R. C. Mucic, *Nature*, 1996, **382**, 607-609.
12. R. J. Macfarlane, B. Lee, H. D. Hill, A. J. Senesi, S. Seifert and C. A. Mirkin, *Proc. Natl. Acad. Sci.*, 2009, **106**, 10493–10498.
13. Z.-G. Wang and B. Ding, *Adv. Mater.*, 2013, **25**, 3905–3914.
14. Y. Zhang, F. Lu, K. G. Yager, D. van der Lelie and O. Gang, *Nature Nanotechnol.*, 2013, **8**, 865–872.

15. J. Sun and R. N. Zuckermann, *ACS Nano*, 2013, **7**, 4715–4732.
16. N. A. Merrill, F. Yan, H. Jin, P. Mu, C.-L. Chen and M. R. Knecht, *Nanoscale*, 2018, **10**, 12445–12452.
17. F. Jiao, X. Wu, T. Jian, S. Zhang, H. Jin, P. He, C.-L. Chen and J. J. De Yoreo, *Angew. Chem. Int. Ed.*, 2019, **58**, 12223–12230.
18. F. Yan, L. Liu, T. R. Walsh, Y. Gong, P. Z. El-Khoury, Y. Zhang, Z. Zhu, J. J. De Yoreo, M. H. Engelhard, X. Zhang and C.-L. Chen, *Nature Commun.*, 2018, **9**, 2327.
19. R. Li, A. Smolyakova, G. Maayan and J. D. Rimer, *Chem. Mater.*, 2017, **29**, 9536–9546.
20. C.-L. Chen, J. Qi, R. N. Zuckermann and J. J. DeYoreo, *J. Am. Chem. Soc.*, 2011, **133**, 5214–5217.
21. X. Ma, S. Zhang, F. Jiao, C. J. Newcomb, Y. Zhang, A. Prakash, Z. Liao, M. D. Baer, C. J. Mundy, J. Pfaendtner, A. Noy, C.-L. Chen and J. J. De Yoreo, *Nature Mater.*, 2017, **16**, 767–774.
22. C.-L Chen, J. H. Qi, J. H. Tao, R. N. Zuckermann, J. J. DeYoreo, *Sci. Rep.,* 2014, **4**, 6266.
23. H. Jin, F. Jiao, M. D. Daily, Y. Chen, F. Yan, Y.-H. Ding, X. Zhang, E. J. Robertson, M. D. Baer and C.-L. Chen, *Nature Commun.*, 2016, **7**, 12252.
24. H. Jin, Y.-H. Ding, M. Wang, Y. Song, Z. Liao, C. J. Newcomb, X. Wu, X.-Q. Tang, Z. Li, Y. Lin, F. Yan, T. Jian, P. Mu and C.-L. Chen, *Nature Commun.*, 2018, **9**, 270.
25. R. V. Mannige, T. K. Haxton, C. Proulx, E. J. Robertson, A. Battigelli, G. L. Butterfoss, R. N. Zuckermann and S. Whitelam, *Nature*, 2015, **526**, 415–420.
26. S. Jin, Y. Hu, Z. Gu, L. Liu and H.-C. Wu, *J. Nanomater.*, 2011, **2011**, 1–13.
27. S. Mazumder, R. Dey, M. K. Mitra, S. Mukherjee and G. C. Das, *J. Nanomater.*, 2009, **2009**, 1–17.
28. L. Zhao, L. Hu and X. Fang, *Adv. Funct. Mater.*, 2012, **22**, 1551–1566.
29. W. Liu, H. S. Choi, J. P. Zimmer, E. Tanaka, J. V. Frangioni and M. Bawendi, *J. Am. Chem. Soc.*, 2007, **129**, 14530–14531.
30. V. H. Chu, T. H. Lien Nghiem, T. H. Le, D. Lam Vu, H. Nhung Tran and T. K. Lien Vu, *Adv. Nat. Sci: Nanosci. Nanotechnol.*, 2012, **3**, 025017.
31. Y. Yuan and M. Krüger, *Polymers*, 2012, **4**, 1–19.
32. A. N. Beecher, X. Yang, J. H. Palmer, A. L. LaGrassa, P. Juhas, S. J. L. Billinge and J. S. Owen, *J. Am. Chem. Soc.*, 2014, **136**, 10645–10653.
33. M. B. Teunis, S. Dolai and R. Sardar, *Langmuir*, 2014, **30**, 7851–7858.
34. A. M. Smith and S. Nie, *Acc. Chem. Res.*, 2010, **43**, 190–200.
35. A. P. Alivisatos, *Science*, 1996, **271**, 933–937.
36. B. M. Cossairt, P. Juhas, S. Billinge and J. S. Owen, *J. Phys. Chem. Lett.*, 2011, **2**, 3075–3080.
37. P. Akkapeddi, S.-A. Azizi, A. M. Freedy, P. M. S. D. Cal, P. M. P. Gois and G. J. L. Bernardes, *Chem. Sci.*, 2016, **7**, 2954–2963.
38. E. Oh, K. Susumu, J. B. Blanco-Canosa, I. L. Medintz, P. E. Dawson and H. Mattoussi, *Small*, 2010, **6**, 1273–1278.
39. C. Srinivasan, J. Lee, F. Papadimitrakopoulos, L. K. Silbart, M. Zhao and D. J. Burgess, *Mol. Ther.*, 2006, **14**, 192–201.
40. B. Zang, J. Yu, C. Liu, J. Wang, H. Han, P. Zhang, D. Shi, *RSC Adv.,* 2016, **6**, 50119–50127.
41. Vera-Hidalgo, E. Giovanelli, C. Navío and E. M. Pérez, *J. Am. Chem. Soc.*, 2019, **141**, 3767–3771.

42. W. J. Parak, D. Gerion, D. Zanchet, A. S. Woerz, T. Pellegrino, C. Micheel, S. C. Williams, M. Seitz, R. E. Bruehl, Z. Bryant, C. Bustamante, C. R. Bertozzi and A. P. Alivisatos, *Chem. Mater.*, 2002, **14**, 2113–2119.

43. A. Banerjee, C. Grazon, B. Nadal, T. Pons, Y. Krishnan and B. Dubertret, *Bioconjugate Chem.*, 2015, **26**, 1582–1589.

44. E. Giovanelli, E. Muro, G. Sitbon, M. Hanafi, T. Pons, B. Dubertret and N. Lequeux, *Langmuir*, 2012, **28**, 15177–15184.

45. W. Liu, H. S. Choi, J. P. Zimmer, E. Tanaka, J. V. Frangioni and M. Bawendi, *J. Am. Chem. Soc.*, 2007, **129**, 14530–14531.

46. G. Hosseinzadeh, A. Maghari, S. M. F. Farniya, A. H. Keihan and A. A. Moosavi-Movahedi, *Mater. Sci. Eng. C*, 2017, **77**, 836–845.

47. D. Bermejo-Velasco, A. Azémar, O. P. Oommen, J. Hilborn and O. P. Varghese, *Biomacromolecules*, 2019, **20**, 1412–1420.

48. Y.-S. Park, A. Dmytruk, I. Dmitruk, A. Kasuya, Y. Okamoto, N. Kaji, M. Tokeshi and Y. Baba, *J. Phys. Chem. C*, 2010, **114**, 18834–18840.

49. Y. Nosaka, N. Ohta, T. Fukuyama and N. Fujii, *J. Coll. Interf. Sci.*, 1993, **155**, 23–29.

50. D. Lawless, S. Kapoor and D. Meisel, *J. Phys. Chem.*, 1995, **99**, 10329–10335.

51. W. C. W. Chan and S. Nie, *Science*, 1998, **281**, 2016–2018.

52. R. R. Knauf, J. C. Lennox and J. L. Dempsey, *Chem. Mater.*, 2016, **28**, 4762–4770.

53. N. C. Anderson, M. P. Hendricks, J. J. Choi and J. S. Owen, *J. Am. Chem. Soc.*, 2013, **135**, 18536–18548.

54. C. F. Brewer and J. P. Riehm, *Anal. Biochem.*, 1967, **18**, 248–255.

55. I. Chambrier, C. Banerjee, S. Remiro-Buenamañana, Y. Chao, A. N. Cammidge and M. Bochmann, *Inorg. Chem.*, 2015, **54**, 7368–7380.

56. T. Kurihara, Y. Noda and K. Takegoshi, *ACS Omega*, 2019, **4**, 3476–3483.

57. J. Zhang, F. Tian, M. Zhang, T. Li, X. Kong, Y. Zhou and N. A. Kotov, *Nanoscale Horiz.*, 2019, **4**, 1416–1424.

58. S. D. Fontaine, R. Reid, L. Robinson, G. W. Ashley and D. V. Santi, *Bioconjugate Chem.*, 2015, **26**, 145–152.

TOC Graphic.

Pre-assembled peptoid tubes and sheets are used as a generalizable platform to template the assembly of controllable densities of CdSe quantum dots and clusters through a robust, covalent linkage.